Editors' Suggestion

Variations in the charge radii of indium isotopes between $N = 52$ and 82

A. R. Vernon,[1,2,3,4,*] C. L. Binnersley,[1] B. K. Sahoo,[5] J. Billowes,[1] M. L. Bissell,[1] T. E. Cocolios,[2] R. P. de Groote,[2,6] G. J. Farooq-Smith,[2] K. T. Flanagan,[1,7] R. F. Garcia Ruiz,[3,8] G. Georgiev,[9] W. Gins,[2] F. P. Gustafsson,[2] R. Heinke,[8] J. D. Holt,[10,11] A. Kanellakopoulos,[2] J. Karthein,[3] Á. Koszorús,[2] D. Leimbach,[12,13] K. M. Lynch,[1,8,†] T. Miyagi,[14] W. Nazarewicz,[15] G. Neyens,[2,8] P.-G. Reinhard,[16] C. M. Ricketts,[1] S. R. Stroberg,[17,18] S. G. Wilkins,[3,12] X. F. Yang,[2,19] and D. T. Yordanov[8,9]

(CRIS-ISOLDE Collaboration)

[1]*Department of Physics and Astronomy, The University of Manchester, Manchester M13 9PL, United Kingdom*
[2]*KU Leuven, Instituut voor Kern- en Stralingsfysica, B-3001 Leuven, Belgium*
[3]*Massachusetts Institute of Technology, Cambridge, Massachusetts 02139, USA*
[4]*Duke University, Durham, North Carolina 27708, USA*
[5]*Atomic, Molecular and Optical Physics Division, Physical Research Laboratory, Navrangpura, Ahmedabad 380009, India*
[6]*Department of Physics, University of Jyväskylä, Survontie 9, Jyväskylä FI-40014, Finland*
[7]*Photon Science Institute Alan Turing Building, University of Manchester, Manchester M13 9PY, United Kingdom*
[8]*EP Department, CERN, CH-1211 Geneva 23, Switzerland*
[9]*IJCLab, CNRS/IN2P3, Université Paris-Saclay, 91405 Orsay, France*
[10]*TRIUMF,4004 Wesbrook Mall, Vancouver, British Columbia V6T 2A3, Canada*
[11]*Department of Physics, McGill University, Montréal, Quebec H3A 2T8, Canada*
[12]*EN Department, CERN, CH-1211 Geneva 23, Switzerland*
[13]*Department of Physics, The University of Gothenburg, Gothenburg, Sweden*
[14]*Center for Computational Sciences, University of Tsukuba, Ibaraki 305-8577, Japan*
[15]*Department of Physics and Astronomy and FRIB Laboratory, Michigan State University, East Lansing, Michigan 48824, USA*
[16]*Institut für Theoretische Physik II, Universität Erlangen-Nürnberg, 91058 Erlangen, Germany*
[17]*Department of Physics and Astronomy, University of Notre Dame, Notre Dame, Indiana 46556, USA*
[18]*Department of Physics, University of Washington, Seattle, Washington 98105, USA*
[19]*School of Physics and State Key Laboratory of Nuclear Physics and Technology, Peking University, Beijing 100871, China*

(Received 2 December 2024; accepted 3 March 2025; published 26 June 2025)

Measurements of the $5p\ ^2P_{3/2} \rightarrow 9s\ ^2S_{1/2}$ and $5p\ ^2P_{1/2} \rightarrow 8s\ ^2S_{1/2}$ transitions in the indium atom, combined with new atomic physics calculations, were used to extract the changes in mean-square nuclear charge radii, $\delta\langle r^2\rangle$, of the indium ($Z = 49$) isotopes $^{101-111}$In, $^{113-123}$In, and $^{125-131}$In. With a proton hole in the closed nuclear shell of $Z = 50$, indium provides a detailed study of the effect of unpaired nucleons adjacent to the proton-shell closure, allowing investigation into the charge radii for isotopes between the two major neutron-shell closures at $N = 50$ and $N = 82$. A study of the variations in charge radii between neighboring isotopes with neutron number (the 'odd-even staggering') is presented and provides further insight and challenges for the theoretical description of the size of proton-hole nuclei. Two nuclear theories, density functional theory and the valence-space in-medium similarity renormalization group method, were employed to interpret the data. The new information obtained in this work provides valuable insights into the successes and shortcomings of the theoretical approaches employed.

DOI: 10.1103/PhysRevC.111.064325

I. INTRODUCTION

The size of the nucleus is a fundamental observable that can be used to challenge and constrain nuclear models. The charge radius, $R_{\rm ch}$, is the measure of the size of the proton distribution of a nucleus, whereby variations in the charge radii have been shown to be sensitive probes of global nuclear properties, nucleon-nucleon interactions [1–5], and signatures of nuclear-shell closures [6–11]. Laser spectroscopy can measure the changes in mean-square charge radii, $\delta\langle r^2\rangle$, as neutrons are added or removed. Local variations in the charge radii can be evaluated by analyzing the alternating relative size of $\langle r^2\rangle$ values between neighboring isotopes [12–15], the 'odd-even staggering' (OES). Significant effort has been dedicated to accurately calculate the charge radii of isotope chains at proton-shell closures, thus providing a test of nuclear models before their application

*Contact author: adam.vernon@duke.edu
†Contact author: kara.lynch@manchester.ac.uk

Published by the American Physical Society under the terms of the Creative Commons Attribution 4.0 International license. Further distribution of this work must maintain attribution to the author(s) and the published article's title, journal citation, and DOI.

to more complex nuclei and nuclear matter in stars [16,17]. Two approaches for accurately calculating the charge radii have proven particularly successful: (i) the 'global' approach of nuclear density functional theory (DFT) [18,19] using realistic energy density functionals, and (ii) quantum many-body methods, such as valence-space in-medium similarity renormalization group (VS-IMSRG) [20,21] employing interactions based on chiral effective field theory [22,23]. The DFT approach can be readily applied across the nuclear chart and has been able to predict global and local variations of charge radii and binding energies [10,14,24,25]. Accurate VS-IMSRG calculations are computationally demanding as they include detailed many-body correlations important for local variations, and have so far been successfully applied to describe the charge radii of medium-mass nuclei with $Z \leqslant 29$ [13,26–28].

A natural progression towards a global description of nuclear charge radii is to take these approaches, which have been tested for light and medium-mass nuclei, and to apply them to heavier odd-Z, semimagic, and open-shell systems. This introduces additional complexity due to the increased number of valence-nucleon correlations. The indium ($Z = 49$) isotopes, with a proton hole in the $Z = 50$ shell closure, provide a relatively simple system for such a study. Furthermore, since odd-Z elements typically have no more than two naturally abundant isotopes, the determination of atomic parameters needed for the extraction of the charge radii using empirical methods is not possible. Instead, the use of high-accuracy atomic calculations is required [29].

This paper presents systematic measurements of charge radii in the indium isotopes, from ^{101}In with $N = 52$ up to the $N = 82$ shell closure at ^{131}In, alongside new atomic physics calculations for the extraction of changes in mean-square charge radii. The measurements were performed using the collinear resonance ionization spectroscopy (CRIS) experiment [30] at the ISOLDE facility at CERN. This paper is part of a series of publications presenting results from these measurements [31–38]. Previous laser spectroscopy work [39] measured charge radii from ^{104}In up to ^{127}In, but was unable to study the weakly-produced ground and isomeric states of several odd-odd indium isotopes. The exotic isotopes near doubly magic $N = 50$ and $N = 82$ are typically produced at low rates (below 1000 ions/s) and in the presence of significant isobaric contamination [40]. This makes experiments challenging and sensitive laser spectroscopy techniques are needed to study these isotopes [41]. The sensitivity of the CRIS technique, along with advances in radioactive isotope production, permitted the measurement of the ground and isomeric states from ^{101}In to ^{131}In (with the exceptions of ^{112}In and ^{124}In) and evaluation of the odd-even staggering up to the shell closure at $N = 82$. This paper presents new data on the isomeric states of the indium isotopes, as well as the odd-odd ground states. The experimental results are compared to DFT calculations, including the Fy(Δr, HFB) energy density functional which has been demonstrated to provide a good description of the even-Z Sn ($Z = 50$) [10] and Cd ($Z = 48$) isotopes [24], and VS-IMSRG calculations, including the recently developed $\mathrm{N^2LO_{GO}}$ interaction [26].

II. METHOD

The charge radii measurements in this study combine data from two separate experiments conducted at the ISOLDE facility [42]. The neutron-deficient indium isotopes ($^{101-115}$In) were produced via reactions of 1.4-GeV protons on a thick lanthanum-carbide target. The neutron-rich indium isotopes ($^{115-131}$In) were produced by neutron-induced fission of ^{238}U within a thick uranium-carbide target. The neutrons were produced through spallation reactions induced by 1.4-GeV protons within a tungsten rod located next to the target [40]. In both experiments, the indium isotopes diffused through the heated target material and were ionized with the ISOLDE resonant ionization laser ion source [43]. The ions were then accelerated to 40 keV, mass separated using the ISOLDE high-resolution mass separator before being cooled and bunched using a gas-filled linear Paul trap [44]. Ion bunches were then extracted, reaccelerated and delivered to the CRIS experiment [41]. Calibration of the high voltage of the linear Paul trap, measured by a potential divider as 39 937(1) V (for the neutron-deficient indium isotopes) and 40 034(1) V (for the neutron-rich indium), determined an ion beam-energy of 39 948(1) eV and 39 985(1) eV, respectively [31–33]. The drift of the ion-beam energy was determined to be about ± 1 eV over the course of each experiment, but continual measurement provided a precision of $\leqslant 0.4$ eV. The indium ions were neutralised with a sodium-filled charge-exchange cell, with an efficiency of up to 60% and a calculated relative atomic population of 37% for the $5p\ ^2P_{1/2}$ ground state and 57% for the $5p\ ^2P_{3/2}$ metastable state [45]. The remaining ion fraction was removed by electrostatic deflectors, and the neutral atom bunch was collinearly overlapped with two pulsed lasers. The first pulsed laser was used for resonant excitation and the second pulsed laser for subsequent nonresonant ionization of excited states. The $5p\ ^2P_{3/2} \rightarrow 9s\ ^2S_{1/2}$ (246.8 nm) and $5p\ ^2P_{1/2} \rightarrow 8s\ ^2S_{1/2}$ (246.0 nm) atomic transitions were driven by frequency-tripled laser light from an injection-locked Ti:Sapphire cavity, seeded with a narrow-band SolsTiS continuous-wave Ti:Sapphire laser and pumped with 532-nm laser light from a Lee Laser LDP-100MQ Nd:YAG. The injection-locked Ti:Sapphire cavity produced pulsed 740-nm laser light (frequency-tripled to produce 246.8-nm light) or 738-nm laser light (frequency-tripled to produce 246.0-nm light) at a repetition rate of 1 kHz and spectral linewidth of 20 MHz [46]. The frequency of the first-step transition was measured with a HighFinesse WSU-2 wavelength meter, which was stabilized using a TOPTICA DLC DL Pro 780 diode laser locked to the $5s\ ^2S_{1/2} \rightarrow 5p\ ^2P_{3/2}$ $F = 2 \rightarrow 3$ transition of ^{87}Rb using a saturated absorption spectroscopy system. A laser fluence of $3\,\mu\mathrm{J/cm^2}$ was used to saturate the transitions [46,47]. The resonantly-excited atoms were photoionized by a 1064-nm laser light pulse of 80(5) mJ and 7-ns duration, produced by a Litron LPY 601 50-100 PIV Nd:YAG laser at 100 Hz. The frequency of the resonant first step was scanned and the resulting ions were deflected onto a detector, producing hyperfine spectra from which hyperfine parameters and isotope-shift values were extracted. The hyperfine structure of the neutron-deficient indium isotopes were analyzed with a Bayesian analysis using the binned

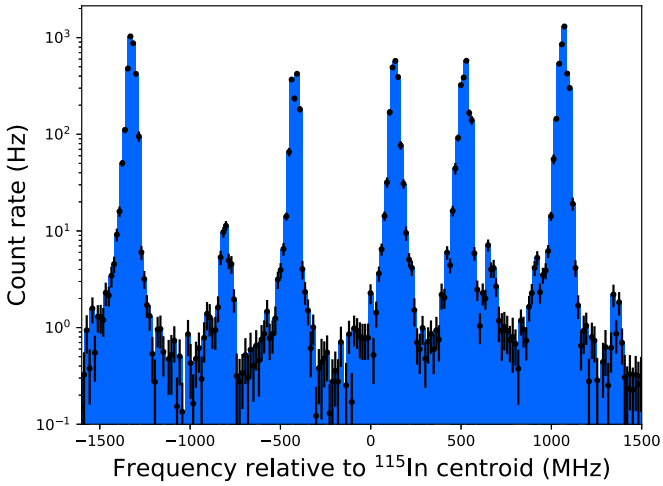

FIG. 1. Hyperfine spectrum of the $5p\ ^2P_{3/2} \rightarrow 9s\ ^2S_{1/2}$ (246.8 nm) transition for ^{114}In, relative to the centroid frequency of the reference isotope, ^{115}In.

maximum likelihood estimation, as described in Ref. [36]. The hyperfine structure of the neutron-rich isotopes were fit with a χ^2-minimization routine, as described in Ref. [31]. Each analysis used a pseudo-Voigt lineshape for the hyperfine spectra, with a typical linewidth between 35–50 MHz [31,33]. The Lorentzian and Gaussian components were typically between 0–10 MHz and 30–50 MHz, respectively. Results were independently verified with parallel analyses [31,33] using the SATLAS package [48]. The laser-excitation processes were performed under ultrahigh vacuum conditions ($< 5 \times 10^{-10}$ mbar), to reduce the collisional ionization process to 1 ion in 10^7 beam particles. This corresponded to a typical background rate of 0.5 ions/second, see Fig. 1. An independent measurement of the yield at mass $A = 130$, performed by the ISOLDE Fast Tape Station [49], measured 1×10^4 ions/s of ^{130}In alongside 1×10^7 ions/s of ^{130}Cs contamination [31].

The isotope shifts, $\delta\nu^{115,A}$, of each isotope A were obtained relative to the reference isotope ^{115}In, which was measured throughout the experiments. Isotope shift values were determined from the weighted average of each individual isotope shift, as described in Refs. [36] and [45]. The changes in mean-square charge radii, $\delta\langle r^2\rangle^{115,A}$, were extracted using the relation

$$\delta\nu^{115,A} = F\delta\langle r^2\rangle^{115,A} + M\frac{m_A - m_{115}}{m_{115}m_A}, \tag{1}$$

where m_A and m_{115} are the atomic masses of the isotopes [50,51], F is the field-shift factor and M is the mass-shift factor. M is the sum of the normal mass shift (K^{NMS}) and the specific mass shift (K^{SMS}). For each atomic transition, the F and M factors were calculated with $F = F_{\mathrm{l}} - F_{\mathrm{u}}$ and $M = M_{\mathrm{l}} - M_{\mathrm{u}}$, where 'l' and 'u' denotes the lower and upper atomic states, respectively.

The newly calculated values for F, K^{NMS} and K^{SMS} factors used extract the charge radii are presented in Table I. Here, we have employed the analytical-response based relativistic coupled-cluster (RCC) theory which was first reported in Ref. [29]. In this approach, the initial wave functions were obtained using the Dirac-Hartree-Fock (DHF) method. Calculations were performed first with a very large basis considering atomic orbitals up to orbital angular momentum $l = 6$ at the singles and doubles approximation in the RCC theory (RCCSD method) [29]. Calculations were then carried out at the singles, doubles and triples approximation in the RCC theory (RCCSDT method) with atomic orbitals

TABLE I. Calculated ionization potential (IP), field-shift factor (F), normal mass shift factor (K^{NMS}), and specific mass shift factor (K^{SMS}) values from different atomic methods. The IP values are compared with experimental values (Expt.) from Ref. [52]. The F, K^{NMS} and K^{SMS} factors are compared with previous calculations [29]. The 'Final' values used to extract the charge radii are presented in bold. Uncertainties are given in parentheses.

Method	$5p\ ^2P_{1/2}$	$5p\ ^2P_{3/2}$	$6s\ ^2S_{1/2}$	$8s\ ^2S_{1/2}$	$9s\ ^2S_{1/2}$
			Ionization potential (IP) (cm^{-1})		
DHF	41507	39506	20572	5816	3835
RCCSD	46612	44410	22291	6031	3949
RCCSDT	46606	44404	22288	6031	3950
+Breit	−54	−20	−6	−1	−1
+QED	18	18	−2	−1	−0
+Basis	140	90	19	3	2
Final	**46710(72)**	**44492(60)**	**22299(20)**	**6032(5)**	**3951(5)**
Expt. [52]	46670	44458	22297	6033	3951
			Field-shift factor (F) ($\mathrm{MHz/fm}^2$)		
DHF	−62.95	−0.02	−413.80	−64.62	−35.39
RCCSD	1466.17	1429.24	−383.24	−57.84	−30.82
RCCSDT	1584.57	1560.18	−337.66	−50.71	−26.26
+Breit	0.12	−2.08	0.31	0.05	0.66
+QED	−9.41	−9.07	1.94	0.28	0.15
+Basis	0.09	1.92	−2.09	−0.30	−0.19
Final	**1575(30)**	**1551(27)**	**−338(8)**	**−51(5)**	**−26(3)**
Ref. [29][a]	1435(6)	1442(6)	−383(1)	−55.9(2.5)	−(5)
			Normal mass shift factor ($30.7K^{\mathrm{NMS}}$) (GHz u)		
DHF	3172.34	2907.98	621.58	139.87	88.55
RCCSD	805.45	782.37	345.92	96.91	62.97
RCCSDT	740.82	727.08	343.87	94.30	61.82
+Breit	2.27	−1.00	−0.12	−0.03	0.03
+QED	1.93	0.19	0.35	0.05	0.70
+Basis	7.06	4.11	1.0	0.16	0.74
Final	**752(20)**	**730(20)**	**345(7)**	**95(5)**	**63(5)**
Ref. [29][a]	774(41)	734(37)	340(5)	96(1)	61.7(5)
Ref. [29][b]	768	731	367	99	65
			Specific mass shift factor (K^{SMS}) (GHz u)		
DHF	−2068.78	−1803.35	−207.60	−32.11	−17.56
RCCSD	−584.34	−480.80	109.58	15.07	7.89
RCCSDT	−409.58	−333.65	145.87	22.25	12.26
+Breit	−1.68	6.77	2.51	0.34	0.14
+QED	0.03	0.85	−0.71	−0.07	−0.03
+Basis	−6.63	−3.58	−0.53	−0.08	−0.03
Final	**−418(70)**	**−330(70)**	**147(30)**	**23(10)**	**12(5)**
Ref. [29][a]	−638(71)	−533(69)	94(26)	13(4)	8.6(5)
Ref. [29][b]	−536(122)	−507(111)	169(51)	24(80)	−13(66)

[a]Theory, Table I, Method 'AR'.
[b]Experiment, Table I.

TABLE II. Ground-state isotope shift ($\delta\nu^{115,A}$) and extracted charge radii ($\delta\langle r^2\rangle^{115,A}$) values for the $5p\ ^2P_{3/2} \rightarrow 9s\ ^2S_{1/2}$ (246.8 nm) and $5p\ ^2P_{1/2} \rightarrow 8s\ ^2S_{1/2}$ (246.0 nm) atomic transitions in the indium isotopes, $^{101-131}$In. Literature charge radii values for the $5p\ ^2P_{3/2} \rightarrow 6s\ ^2S_{1/2}$ (451 nm) and $5p\ ^2P_{1/2} \rightarrow 6s\ ^2S_{1/2}$ (410 nm) atomic transitions, recalculated using new atomic factors, are presented for comparison [39]. The atomic F and M factors used to extract the charge radii are given in Table I. Statistical uncertainties (from experimental measurements) are given in parenthesis and systematic uncertainties (from atomic theory calculations) are given in square brackets.

		$\delta\nu^{115,A}$ (MHz)		$\delta\langle r^2\rangle^{115,A}$ (fm^2)			
		$5p\ ^2P_{3/2}$ $\rightarrow 9s\ ^2S_{1/2}$	$5p\ ^2P_{1/2}$ $\rightarrow 8s\ ^2S_{1/2}$	$5p\ ^2P_{3/2}$ $\rightarrow 9s\ ^2S_{1/2}$	$5p\ ^2P_{1/2}$ $\rightarrow 8s\ ^2S_{1/2}$	$5p\ ^2P_{3/2}$ $\rightarrow 6s\ ^2S_{1/2}$	$5p\ ^2P_{1/2}$ $\rightarrow 6s\ ^2S_{1/2}$
A	I	(This work)	(This work)	(This work)	(This work)	(Ref. [39])	(Ref. [39])
101	$(9/2^+)$	−2401(7)[a]	−2417(10)[a]	−1.274(5)[60][a]	−1.326(6)[60][a]		
102	(6^+)	−2206(10)	−2199(12)	−1.171(7)[55]	−1.205(8)[55]		
103	$(9/2^+)$	−1936(13)[a]	−1933(9)[a]	−1.019(8)[50][a]	−1.054(6)[50][a]		
104	(6^+)	−1749(12)	−1757(9)	−0.919(8)[46]	−0.958(6)[45]	−0.937(18)[41]	
105	$9/2^+$	−1524(13)[a]	−1512(8)[a]	−0.795(8)[41][a]	−0.820(5)[41][a]	−0.816(15)[37]	
106	7^+	−1372(13)	−1387(11)	−0.718(8)[36]	−0.755(7)[36]	−0.755(13)[33]	
107	$9/2^+$	−1168(18)[a]	−1133(19)[a]	−0.607(11)[32][a]	−0.610(12)[32][a]	−0.640(11)[29]	
108	7^+	−1039(12)	−1042(10)	−0.543(8)[28]	−0.566(6)[28]	−0.563(5)[25]	−0.575(12)[25]
109	$9/2^+$	−838(10)[a]	−840(5)[a]	−0.433(7)[23][a]	−0.453(3)[23][a]	−0.457(7)[21]	
110	7^+	−739(18)		−0.387(12)[20]		−0.401(9)[18]	
111	$9/2^+$	−538(19)[a]	−550(7)[a]	−0.277(12)[15][a]	−0.297(5)[15][a]	−0.289(11)[14]	−0.307(4)[14]
112	1^+						
113	$9/2^+$	−264(10)[a]	−271(25)[a]	−0.136(6)[8][a]	−0.146(15)[8][a]	−0.143(0)[7]	−0.148(2)[7]
114	1^+	−188(7)		−0.103(4)[4]			
115	$9/2^+$	0	0	0	0	0	0
116	1^+	+106(20)		+0.052(13)[4]			
117	$9/2^+$	+265(3)[a]	+243(5)[a]	+0.137(2)[7][a]	+0.130(3)[7][a]	+0.131(3)[7]	+0.139(4)[7]
118	1^+	+333(3)	+334(6)	+0.165(2)[11]	+0.176(4)[11]		
119	$9/2^+$	+475(3)[a]		+0.241(2)[14][a]		+0.248(3)[13]	+0.254(4)[13]
120	1^+	+571(9)	+551(6)	+0.287(6)[18]	+0.291(4)[17]		
121	$9/2^+$	+654(2)[a]		+0.326(1)[21][a]		+0.344(3)[19]	+0.357(3)[19]
122	1^+	+710(8)	+728(7)	+0.347(5)[24]	+0.381(4)[24]		
123	$(9/2)^+$	+756(3)[a]		+0.363(2)[27][a]		+0.433(3)[25]	+0.451(4)[25]
124	$(3)^+$					+0.461(6)[27]	+0.486(7)[27]
125	$9/2^+$	+941(4)[a]		+0.453(3)[33][a]		+0.508(6)[30]	+0.532(4)[30]
126	$3^{(+)}$	+1026(3)		+0.494(2)[36]		+0.536(6)[33]	+0.570(12)[33]
127	$(9/2^+)$	+1129(4)[a]	+1115(5)[a]	+0.546(3)[39][a]	+0.576(3)[39][a]	+0.570(7)[36]	
128	$(3)^+$	+1147(3)	+1147(9)	+0.545(2)[42]	+0.588(6)[42]		
129	$(9/2^+)$	+1251(2)[a]	+1254(5)[a]	+0.598(1)[45][a]	+0.646(3)[45][a]		
130	$1^{(-)}$	+1340(3)	+1324(8)	+0.642(2)[48]	+0.681(5)[47]		
131	$(9/2^+)$	+1364(4)[a]		+0.645(3)[51][a]			

[a]Values published in Ref. [36] but included here for completeness.

up to $l = 6$. Higher-order relativistic corrections from the Breit (labeled as '+Breit') and QED (labeled as '+QED') effects were estimated for the RCCSD method. To aid understanding, Table I presents results from the smaller basis using the DHF and RCCSD method explicitly, in addition to the differences between the values from the smaller and larger basis functions, listed as '+Basis'. For completeness and verifying the reliability of the calculations, the ionization potentials (IPs) of the respective valence electrons from several states are presented and compared to the experimental values [52]. The 'final' values in bold, used to calculate the charge radii, are taken as the total results from the RCCSDT method along with the Breit, QED and Basis corrections. Results differ from those listed in Ref. [29] mostly due to large contributions arising from the triple excitations. The uncertainties in the calculated values are larger than those quoted in Ref. [36], due to neglected contributions from quadrupole excitations. Re-analysis of the uncertainties using triple excitation operator amplitudes allowed extrapolation of these quadrupole-excitations contributions, which resulted in larger uncertainties.

III. RESULTS

The measured isotope shift values, $\delta\nu^{115,A}$, determined from the hyperfine spectra, and extracted charge radii differences, $\delta\langle r^2\rangle^{115,A}$, for the $5p\ ^2P_{3/2} \rightarrow 9s\ ^2S_{1/2}$ (246.8 nm) and $5p\ ^2P_{1/2} \rightarrow 8s\ ^2S_{1/2}$ (246.0 nm) atomic transitions are presented in Tables II and III. Values for the ground states and isomeric states are presented in Tables II and III, respectively. The values for the ground states of the odd-even indium isotopes are published in Ref. [36] and the high-spin states of

TABLE III. Isomeric-state isotope shift ($\delta\nu^{115,A}$) and extracted charge radii ($\delta\langle r^2\rangle^{115,A}$) values for the $5p\ ^2P_{3/2} \rightarrow 9s\ ^2S_{1/2}$ (246.8 nm) and $5p\ ^2P_{1/2} \rightarrow 8s\ ^2S_{1/2}$ (246.0 nm) atomic transitions in the indium isotopes, $^{101-131}$In. Literature charge radii values for the $5p\ ^2P_{3/2} \rightarrow 6s\ ^2S_{1/2}$ (451 nm) and $5p\ ^2P_{1/2} \rightarrow 6s\ ^2S_{1/2}$ (410 nm) atomic transitions, recalculated using new atomic factors, are presented for comparison [39]. The atomic F and M factors used to extract the charge radii are given in Table I. Statistical uncertainties (from experimental measurements) are given in parenthesis and systematic uncertainties (from atomic theory calculations) are given in square brackets.

		$\delta\nu^{115,A}$ (MHz)		$\delta\langle r^2\rangle^{115,A}$ (fm^2)			
A	I	$5p\ ^2P_{3/2} \rightarrow 9s\ ^2S_{1/2}$ (This work)	$5p\ ^2P_{1/2} \rightarrow 8s\ ^2S_{1/2}$ (This work)	$5p\ ^2P_{3/2} \rightarrow 9s\ ^2S_{1/2}$ (This work)	$5p\ ^2P_{1/2} \rightarrow 8s\ ^2S_{1/2}$ (This work)	$5p\ ^2P_{3/2} \rightarrow 6s\ ^2S_{1/2}$ (Ref. [39])	$5p\ ^2P_{1/2} \rightarrow 6s\ ^2S_{1/2}$ (Ref. [39])
101	$(1/2^-)$	−2434(10)	−2512(15)	−1.295(6)[60]	−1.385(9)[60]		
103	$(1/2^-)$	−1948(13)	−1959(9)	−1.027(8)[50]	−1.070(6)[50]		
104	(3^+)	−1748(12)	−1790(9)	−0.919(8)[46]	−0.979(6)[46]		
105	$(1/2^-)$	−1507(13)	−1520(14)	−0.785(8)[41]	−0.824(9)[41]		
106	$(2)^+$	−1426(13)	−1374(11)	−0.752(8)[37]	−0.746(7)[36]		
107	$1/2^-$	−1128(18)	−1121(19)	−0.581(11)[32]	−0.603(12)[32]		
108	2^+	−1023(12)	−1031(10)	−0.532(8)[28]	−0.559(6)[28]	−0.558(5)[25]	−0.563(19)[25]
109	$1/2^-$	−776(11)	−791(5)	−0.393(7)[23]	−0.423(3)[23]		
110	2^+	−739(18)		−0.387(12)[20]			
111	$1/2^-$	−478(19)	−493(10)	−0.239(12)[15]	−0.262(6)[15]		
112	4^+					−0.243(1)[10]	
113	$1/2^-$	−211(13)	−223(25)	−0.102(8)[7]	−0.117(15)[7]		
114	5^+	−171(10)	−175(5)	−0.093(6)[4]	−0.097(3)[4]	−0.097(1)[4]	−0.099(3)[4]
115	$1/2^-$	+54(5)	+26(8)	+0.034(3)[0]	+0.016(5)[0]	+0.015(3)[0]	
116	5^+	+99(2)	+89(5)	+0.047(1)[4]	+0.045(3)[4]	+0.054(1)[3]	+0.057(2)[3]
116	8^-	+99(20)	+86(8)	+0.047(13)[4]	+0.043(5)[4]	+0.049(1)[3]	+0.053(3)[3]
117	$1/2^-$	+283(4)	+265(5)	+0.149(3)[7]	+0.143(3)[7]	+0.140(6)[7]	
118	5^+	+329(2)	+330(5)	+0.163(1)[11]	+0.174(3)[11]	+0.176(2)[10]	+0.182(2)[10]
118	8^-	+324(3)	+324(5)	+0.160(2)[11]	+0.170(3)[11]	+0.171(2)[10]	+0.179(2)[10]
119	$1/2^-$	+487(4)		+0.248(3)[14]		+0.248(3)[14]	
120	$(5)^+$	+556(5)	+531(5)	+0.278(3)[18]	+0.278(3)[17]	+0.282(3)[16]	+0.295(2)[16]
120	(8^-)	+530(2)	+500(5)	+0.261(1)[17]	+0.259(3)[17]	+0.276(2)[16]	+0.282(2)[16]
121	$1/2^-$	+661(3)		+0.330(2)[21]		+0.341(3)[19]	
122	5^+	+674(5)	+704(5)	+0.324(3)[24]	+0.367(3)[24]	+0.375(4)[22]	+0.389(4)[22]
122	(8^-)	+658(8)	+687(5)	+0.314(5)[24]	+0.356(3)[24]	+0.374(4)[22]	+0.384(3)[22]
123	$(1/2)^-$	+753(3)		+0.361(2)[27]		+0.425(4)[25]	
124	(8^-)					+0.460(3)[27]	+0.472(6)[27]
125	$1/2^{(-)}$	+926(5)		+0.443(3)[33]		+0.500(5)[30]	
126	(8^-)	+1019(5)		+0.489(3)[36]		+0.539(4)[33]	+0.566(4)[33]
127	$(1/2^-)$	+1114(3)	+1098(5)	+0.537(2)[39]	+0.566(3)[39]		
127	$(21/2^-)$	+1110(3)[a]	+1086(5)[a]	+0.534(2)[39][a]	+0.558(3)[39][a]		
128	(8^-)	+1127(4)	+1101(7)	+0.532(3)[42]	+0.559(4)[41]		
129	$(1/2^-)$	+1231(4)	+1233(6)	+0.586(3)[45]	+0.633(4)[44]		
129	$(23/2^-)$	+1171(2)[a]	+1167(5)[a]	+0.548(1)[45][a]	+0.592(3)[44][a]		
130	(5^+)	+1281(3)	+1253(6)	+0.605(2)[48]	+0.637(4)[47]		
130	(10^-)	+1305(3)	+1289(5)	+0.620(2)[48]	+0.659(3)[47]		
131	$(1/2^-)$	+1366(3)	+1366(9)	+0.647(2)[51]	+0.699(6)[50]		

[a]Values published in Ref. [37] but included here for completeness.

^{127}In and ^{129}In are published in Ref. [37] and are included for completeness. These values are compared to literature charge radii values, extracted from $\delta\nu^{115,A}$ of the $5p\ ^2P_{3/2} \rightarrow 6s\ ^2S_{1/2}$ (451 nm) and $5p\ ^2P_{1/2} \rightarrow 6s\ ^2S_{1/2}$ (410 nm) atomic transitions from Ref. [39], and recalculated using the new calculations of atomic parameters presented in this work. The new values agree with those of literature within experimental (statistical) and atomic-factor (systematic) uncertainties.

A comparison between experimental charge radii values and theoretical calculations is shown in Fig. 2. An absolute charge radius value of $R_{\rm ch} = 4.6156(26)$ fm^2 for the reference isotope ^{115}In [53] was used to provide an absolute scale for comparison with theoretical calculations.

The DFT calculations were carried out using three energy density functionals: the Skyrme functional SV-min [54] and the Fayans (Fy) functionals, Fy(Δr, HFB) [2] and the

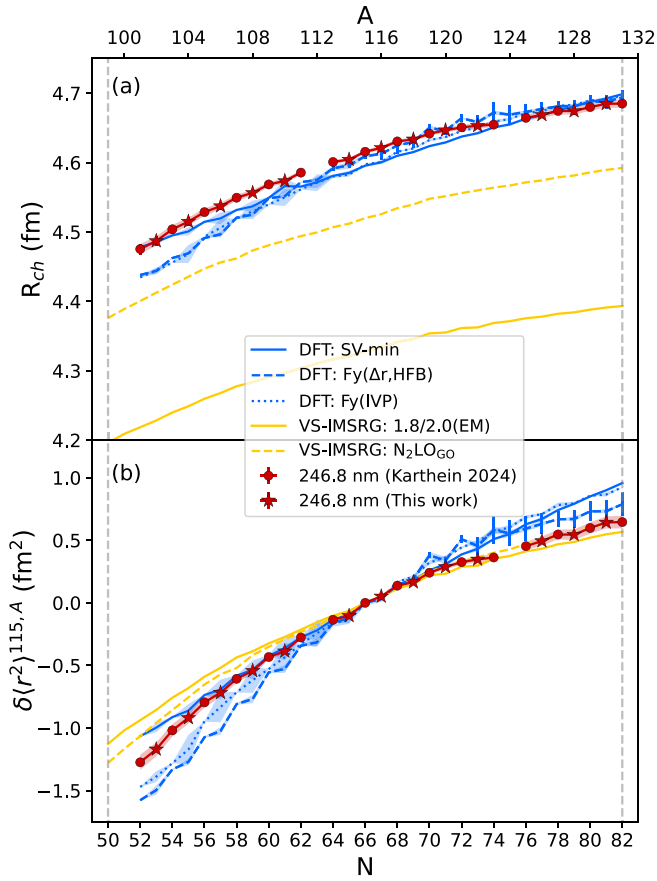

FIG. 2. Comparison of experimental (data markers) and theoretical (lines) values for (a) absolute charge radii, $R_{\rm ch}$, of $^{101-131}$In, and (b) changes in mean-square charge radii, $\delta\langle r^2\rangle^{115,A}$, of $^{101-131}$In relative to ^{115}In. Ground states with recently published (Karthein 2024: Ref. [36]) and newly measured charge radii for the 246.8-nm atomic transition are plotted as circles and stars, respectively.

recently calibrated Fy(IVP) [36]. The parametrization SV-min is calibrated to a large dataset of ground-state properties in semimagic nuclei. The parametrization Fy(Δr, HFB) is based on the same data set plus additional information from the differential radii of the Ca ($Z = 20$) isotopes. The most recent parametrization Fy(IVP) contains isovector pairing and is additionally calibrated to differential radii in Sn ($Z = 50$) and Pb ($Z = 82$) isotopes. In particular, the gradient term in the Fayans pairing functional was found to be essential for reproducing differential radii in the Ca isotopes and near the doubly magic ($N = 82$, $Z = 50$) shell closure of Sn [10]. By a statistical interpretation of the χ^2 fits, statistical uncertainties on the predicted observables were deduced [54,55]. Calculations were performed for both odd-even and odd-odd nuclei using the axial solver `SkyAx` [56] in an extended version which can run the Hartree-Fock-Bogoliubov (HFB) method and allows for odd nuclei. Values were computed by blocking pairing for the odd nucleons with given angular momentum projection Ω on the third axis. These calculations were prone to a systematic error due to approximate angular momentum projection. It was ignored for odd-even isotopes as these nuclei stay close to the spherical shape. For odd-odd isotopes, it was approximated by incoherent averaging over configurations having the same $\Omega = \Omega_p + \Omega_n$. The projection error on radii is negligible for odd-even isotopes and small for odd-odd ones where it amounts to about 0.001–0.002 fm for neutron-rich nuclei and up to 0.004 fm for proton-rich nuclei. Another systematic error comes from sizable collective ground state correlations due to quadrupole softness in the proton-rich region. These tend to enhance radii up to 0.014 fm for proton-rich Sn isotopes [57]. We therefore note that pure DFT predictions become less reliable on the proton-rich side.

Multishell VS-IMSRG calculations [58] were performed using the 1.8/2.0(EM) interaction [59,60], derived from chiral effective field theory and constrained by few-body data. The recently developed N^{2}LO$_{\rm GO}$ interaction was also used. This interaction explicitly includes contributions from the Δ resonance and is constrained to reproduce saturation properties of nuclear matter [26]. For both interactions, three-nucleon forces between valence nucleons are included via ensemble normal ordering [61]. A harmonic oscillator basis of 15 major shells with frequency $\hbar\omega = 16$ MeV was used with a large cut on storage of 3N force matrix elements $e_1 + e_2 + e_3 \leqslant E_{3\rm max} = 24$ [62] was imposed, sufficient to converge calculations of charge radii. Note that in a sufficiently large single-particle space, results are independent of $\hbar\omega$.

IV. DISCUSSION

The experimental results for the absolute charge radii of $^{101-111}$In, $^{113-123}$In, and $^{125-131}$In are compared to the theoretical calculations in Fig. 2(a). For the experimental radii, statistical uncertainties are shown by error bars and systematic uncertainties are shown by shaded areas. The uncertainties for the DFT predictions are about the same for all three functionals and are shown for Fy(Δr,HFB) only to keep the figure readable. The charge radii from all three DFT functionals reproduce the magnitude of the experimental absolute charge radii, whereas both VS-IMSRG models significantly underestimate the measured charge radii [13]. However, the more recent N^{2}LO$_{\rm GO}$ interaction, developed to reproduce nuclear saturation density, represents a significant improvement compared to the traditional 1.8/2.0(EM) interaction [3].

Details of the trends are better seen for differential radii. To that end, the experimental changes in mean-square charge radii, $\delta\langle r^2\rangle^{115,A}$, are shown alongside the theoretical predictions in Fig. 2(b). The Fayans functionals reproduce the slopes at the neutron midshell rather well, but become too steep on the neutron-deficient and neutron-rich sides (which may be improved somewhat by ground-state correlations). SV-min shows a too small slope throughout. Similar behavior had been seen previously for the Sn chain [25].

By contrast, the VS-IMSRG calculations underestimate the slope of the differential radii, but provide a good agreement for the neutron-rich isotopes. The divergence from the experimental neutron-deficient measurements may be attributed to missing collective correlation effects such as quadrupole deformation, which presently pose a computational challenge for VS-IMSRG calculations [35,63,64].

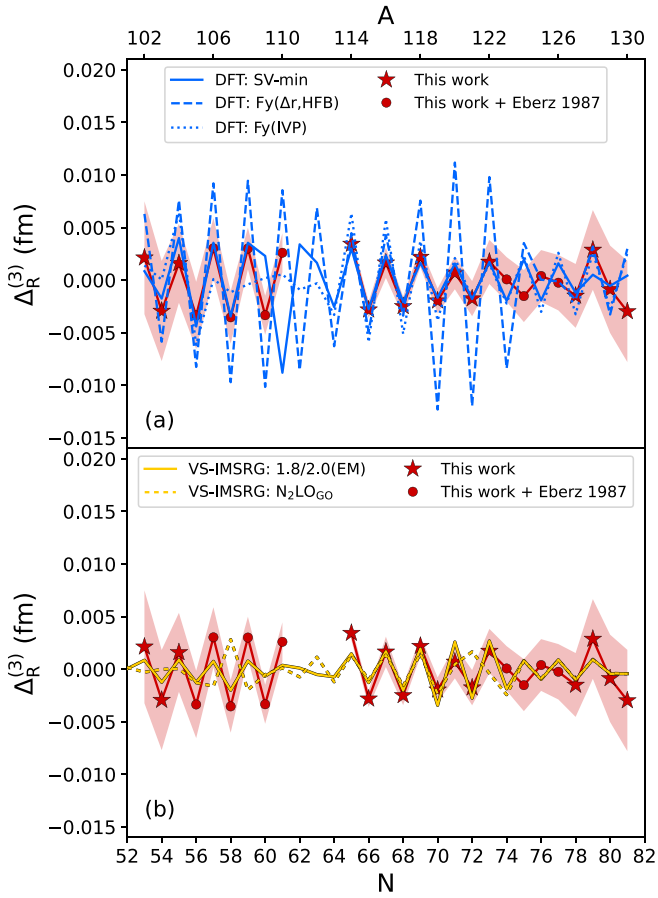

FIG. 3. Odd-even staggering plots comparing experimental values of $\Delta_R^{(3)}$ with (a) DFT calculations and (b) VS-IMSRG calculations for indium. $\Delta_R^{(3)}$ is calculated from the weighted average of the charge radii from four atomic transitions: 246.8 nm and 246.0 nm from this work (stars) and 451 nm and 410 nm from Eberz 1987: Ref. [39] (circles), as given in Table II. The red shaded area represents the combined statistical and systematic weighted uncertainty.

The role of nuclear shell effects on $R_{\rm ch}$ can also be studied through the odd-even staggering (OES) parameter, $\Delta_R^{(3)}$, defined as [13]

$$\Delta_R^{(3)} = \tfrac{1}{2}\left(R_{\rm ch}^{A+1} - 2R_{\rm ch}^{A} + R_{\rm ch}^{A-1}\right). \quad (2)$$

New measurements of the charge radii of the ground states of the odd-odd indium isotopes from $A = 101$ to 131, presented in Table II, allow for the determination of $\Delta_R^{(3)}$ across the indium chain. Figure 3 presents comparison of the experimental $\Delta_R^{(3)}$ values with (a) DFT and (b) VS-IMSRG calculations. The experimental $\Delta_R^{(3)}$ values were calculated from the weighted average of the available charge radii for the 246.8-nm, 246.0-nm, 451-nm, and 410-nm transitions, given in Table II. The weighted average charge radii were calculated using both the statistical (from experimental measurements) and systematic (from atomic theory calculations) uncertainties for each transition. We note that each experimental $\Delta_R^{(3)}$ value can scatter independently within the red shaded area of Fig. 3.

For the discussion of odd-even staggering, we recall that the systematic error on DFT results are significant. We thus concentrate on global trends and less on details. The $\Delta_R^{(3)}$ is well reproduced by SV-min in the regions $N = 53$–59 and $N = 65$–73. Fy(IVP) does well for $N = 53$–56 and also in the region $N = 65$–73. The model Fy(Δr,HFB) overestimates $\Delta_R^{(3)}$ throughout, as discussed in Refs. [3,13]. While the VS-IMSRG calculations also reproduce the midshell $\Delta_R^{(3)}$ behavior, they predict a reduced staggering for the neutron-deficient isotopes. The inversion in $\Delta_R^{(3)}$ at $N = 75$ and $N = 81$, and a reduction in the magnitude of $\Delta_R^{(3)}$ between $N = 75$–78, compared to the rest of the isotopic chain, is not reproduced by any theoretical calculation. However, the magnitude of $\Delta_R^{(3)}$ does decreases in VS-IMSRG. Both SV-min and VS-IMSRG 1.8/2.0(EM) calculations predict an inversion in $\Delta_R^{(3)}$ within the missing experimental data region of $^{111-113}$In. This calls for future measurements of ^{112}In and ^{124}In with the 246.8-nm atomic transition, in order to provide further insights into the structure of these isotopes.

V. CONCLUSION

This work reports the mean-square charge radii of the indium isotopes $^{101-111,113-123,125-131}$In, from $N = 52$ up to the neutron-shell closure at $N = 82$. New measurements of the charge radii of the ground states of ^{102,114,116,118,120,122,128,130}In and the isomeric states of $^{101,103-107,109-111,127-131}$In are presented. The measurements reveal intricate variations in the odd-even staggering of the nuclear charge radii. The constancy of the proton-hole orbital through the indium chain provide an opportunity to study the combined effect of an unpaired proton and unpaired neutron from near the $N = 50$ to the $N = 82$ neutron-shell closures. The SV-min and Fy(IVP) functionals reproduce both the magnitude of the absolute charge radii and the odd-even staggering of the indium isotopes. While the VS-IMSRG calculations fail to reproduce the magnitude of the absolute charge radii, they describe the local variations in charge radii relatively well, especially for the neutron-rich isotopes. All theoretical models fail to reproduce the inversion in odd-even staggering of the charge radii at $N = 75$ and $N = 81$. The results presented here show that the effect of the proton hole can provide valuable insight into the successes and shortcomings of both theoretical approaches used in our study. The shortcomings have a positive effect: they give us direction for the next developmental steps. For DFT, the next step is the generalization of the surface Fayans functional by adding the isovector surface term, as suggested in Ref. [65], and implementation of a more detailed angular momentum projection for odd-odd nuclei that will help reduce the systematic error.

ACKNOWLEDGMENTS

We would like to thank the ISOLDE technical group for their support and assistance, the University of Jyväskylä for the use of the injection-locked cavity, and the Physikalisch-Technische Bundesanstalt (PTB) for the use of their voltage divider. This work was supported by ERC Consolidator Grant No. 648381 (FNPMLS); STFC Grants No. ST/L005794/1, No. ST/L005786/1,

No. ST/P004423/1, No. ST/V001116/1 and Ernest Rutherford Grant No. ST/L002868/1; BOF 14/22/104 from KU Leuven, BriX Research Program No. P7/12; the FWO-Vlaanderen (Belgium); the European Union's Horizon 2020 research and innovation programme under Grant Agreement No. 654002 (ENSAR2); The U.S. Department of Energy, Office of Science, Office of Nuclear Physics under Award No. DE-SC0021176 and No. DE-SC0013365, and DE-SC0023175 (Office of Advanced Scientific Computing Research and Office of Nuclear Physics, Scientific Discovery through Advanced Computing); National Key R&D Program of China (Contract No. 2023YFA1606403), the National Natural Science Foundation of China (No. 12027809); and JST ERATO Grant No. JPMJER2304, Japan. For the VS-IMSRG calculations, the `NuHamil`, `IMSRG++`, and `KSHELL` codes were used to generate chiral EFT matrix elements, to perform the valence-space decoupling, and to solve the valence-space problems, respectively. Part of the VS-IMSRG calculations was performed with an allocation of computing resources on Cedar at WestGrid and Compute Canada. P.-G.R. acknowledges supply of computing resources from the RRZE of the university Erlangen. B.K.S. acknowledges supports from ANRF with Grant No. CRG/2023/002558 and Department of Space, Government of India to carry out his work, and use of ParamVikram-1000 HPC facility at Physical Research Laboratory (PRL), Ahmedabad, for carrying out the atomic calculations. J.K. acknowledges support from a Feodor-Lynen postdoctoral Research Fellowship of the Alexander-von-Humboldt Foundation. K.M.L. acknowledges support from the Royal Society Grant No. DHF \R1\231007 and UK Research and Innovation (UKRI) under the UK government's Horizon Europe funding Guarantee Grant No. EP/Y036816/1 (ESPEN).

DATA AVAILABILITY

The data that support the findings of this article are openly available [66–68].

[1] A. Ekström and G. Hagen, Phys. Rev. Lett. **123**, 252501 (2019).
[2] A. J. Miller, K. Minamisono, A. Klose, D. Garand, C. Kujawa, J. D. Lantis, Y. Liu, B. Maaß, P. F. Mantica, W. Nazarewicz, W. Nörtershäuser, S. V. Pineda, P. G. Reinhard, D. M. Rossi, F. Sommer, C. Sumithrarachchi, A. Teigelhöfer, and J. Watkins, Nat. Phys. **15**, 432 (2019).
[3] Á. Koszorús, X. F. Yang, W. G. Jiang, S. J. Novario, S. W. Bai, J. Billowes, C. L. Binnersley, M. L. Bissell, T. E. Cocolios, B. S. Cooper, R. P. de Groote, A. Ekström, K. T. Flanagan, C. Forssén, S. Franchoo, R. F. Ruiz, F. P. Gustafsson, G. Hagen, G. R. Jansen, A. Kanellakopoulos, M. Kortelainen, W. Nazarewicz, G. Neyens, T. Papenbrock, P. G. Reinhard, C. M. Ricketts, B. K. Sahoo, A. R. Vernon, and S. G. Wilkins, Nat. Phys. **17**, 439 (2021).
[4] R. F. Garcia Ruiz, M. L. Bissell, K. Blaum, A. Ekström, N. Frömmgen, G. Hagen, M. Hammen, K. Hebeler, J. D. Holt, G. R. Jansen, M. Kowalska, K. Kreim, W. Nazarewicz, R. Neugart, G. Neyens, W. Nörtershäuser, T. Papenbrock, J. Papuga, A. Schwenk, J. Simonis, K. A. A. Wendt, and D. T. Yordanov, Nat. Phys. **12**, 594 (2016).
[5] R. An, X. Jiang, L.-G. Cao, and F.-S. Zhang, Chin. Phys. C **46**, 064101 (2022).
[6] R. F. Garcia Ruiz and A. R. Vernon, Eur. Phys. J. A **56**, 136 (2020).
[7] X. Yang, S. Wang, S. Wilkins, and R. G. Ruiz, Prog. Part. Nucl. Phys. **129**, 104005 (2023).
[8] M. Reponen, R. P. de Groote, L. Al Ayoubi, O. Beliuskina, M. L. Bissell, P. Campbell, L. Cañete, B. Cheal, K. Chrysalidis, C. Delafosse, A. de Roubin, C. S. Devlin, T. Eronen, R. F. Garcia Ruiz, S. Geldhof, W. Gins, M. Hukkanen, P. Imgram, A. Kankainen, M. Kortelainen, Á. Koszorús, S. Kujanpää, R. Mathieson, D. A. Nesterenko, I. Pohjalainen, M. Vilén, A. Zadvornaya, and I. D. Moore, Nat. Commun. **12**, 4596 (2021).
[9] T. Day Goodacre, A. V. Afanasjev, A. E. Barzakh, B. A. Marsh, S. Sels, P. Ring, H. Nakada, A. N. Andreyev, P. Van Duppen, N. A. Althubiti, B. Andel, D. Atanasov, J. Billowes, K. Blaum, T. E. Cocolios, J. G. Cubiss, G. J. Farooq-Smith, D. V. Fedorov, V. N. Fedosseev, K. T. Flanagan, L. P. Gaffney, L. Ghys, M. Huyse, S. Kreim, D. Lunney, K. M. Lynch, V. Manea, Y. Martinez Palenzuela, P. L. Molkanov, M. Rosenbusch, R. E. Rossel, S. Rothe, L. Schweikhard, M. D. Seliverstov, P. Spagnoletti, C. Van Beveren, M. Veinhard, E. Verstraelen, A. Welker, K. Wendt, F. Wienholtz, R. N. Wolf, A. Zadvornaya, and K. Zuber, Phys. Rev. Lett. **126**, 032502 (2021).
[10] C. Gorges, L. V. Rodríguez, D. L. Balabanski, M. L. Bissell, K. Blaum, B. Cheal, R. F. Garcia Ruiz, G. Georgiev, W. Gins, H. Heylen, A. Kanellakopoulos, S. Kaufmann, M. Kowalska, V. Lagaki, S. Lechner, B. Maaß, S. Malbrunot-Ettenauer, W. Nazarewicz, R. Neugart, G. Neyens, W. Nörtershäuser, P. G. Reinhard, S. Sailer, R. Sánchez, S. Schmidt, L. Wehner, C. Wraith, L. Xie, Z. Y. Xu, X. F. Yang, and D. T. Yordanov, Phys. Rev. Lett. **122**, 192502 (2019).
[11] K. Kreim, M. Bissell, J. Papuga, K. Blaum, M. De Rydt, R. Garcia Ruiz, S. Goriely, H. Heylen, M. Kowalska, R. Neugart, G. Neyens, W. Nörtershäuser, M. Rajabali, R. Sánchez Alarcón, H. Stroke, and D. Yordanov, Phys. Lett. B **731**, 97 (2014).
[12] S. Kaufmann, J. Simonis, S. Bacca, J. Billowes, M. L. Bissell, K. Blaum, B. Cheal, R. F. Garcia Ruiz, W. Gins, C. Gorges, G. Hagen, H. Heylen, A. Kanellakopoulos, S. Malbrunot-Ettenauer, M. Miorelli, R. Neugart, G. Neyens, W. Nörtershäuser, R. Sánchez, S. Sailer, A. Schwenk, T. Ratajczyk, L. V. Rodríguez, L. Wehner, C. Wraith, L. Xie, Z. Y. Xu, X. F. Yang, and D. T. Yordanov, Phys. Rev. Lett. **124**, 132502 (2020).
[13] R. P. de Groote, J. Billowes, C. L. Binnersley, M. L. Bissell, T. E. Cocolios, T. Day Goodacre, G. J. Farooq-Smith, D. V. Fedorov, K. T. Flanagan, S. Franchoo, R. F. Garcia Ruiz, W. Gins, J. D. Holt, Á. Koszorús, K. M. Lynch, T. Miyagi, W. Nazarewicz, G. Neyens, P.-G. Reinhard, S. Rothe, H. H. Stroke, A. R. Vernon, K. D. A. Wendt, S. G. Wilkins, Z. Y. Xu, and X. F. Yang, Nat. Phys. **16**, 620 (2020).
[14] P. G. Reinhard and W. Nazarewicz, Phys. Rev. C **95**, 064328 (2017).
[15] U. C. Perera, A. V. Afanasjev, and P. Ring, Phys. Rev. C **104**, 064313 (2021).

[16] G. Hagen, A. Ekström, C. Forssén, G. R. Jansen, W. Nazarewicz, T. Papenbrock, K. A. Wendt, S. Bacca, N. Barnea, B. Carlsson, C. Drischler, K. Hebeler, M. Hjorth-Jensen, M. Miorelli, G. Orlandini, A. Schwenk, and J. Simonis, Nat. Phys. **12**, 186 (2016).

[17] J. Erler, N. Birge, M. Kortelainen, W. Nazarewicz, E. Olsen, A. M. Perhac, and M. Stoitsov, Nature **486**, 509 (2012).

[18] M. Bender, P. H. Heenen, and P. G. Reinhard, Rev. Mod. Phys. **75**, 121 (2003).

[19] N. Schunck, *Energy Density Functional Methods for Atomic Nuclei* (IOP Publishing, Bristol, 2019).

[20] S. R. Stroberg, H. Hergert, S. K. Bogner, and J. D. Holt, Annu. Rev. Nucl. Part. Sci. **69**, 307 (2019).

[21] S. R. Stroberg, J. D. Holt, A. Schwenk, and J. Simonis, Phys. Rev. Lett. **126**, 022501 (2021).

[22] E. Epelbaum, H.-W. Hammer, and U.-G. Meißner, Rev. Mod. Phys. **81**, 1773 (2009).

[23] R. Machleidt and D. R. Entem, Phys. Rep. **503**, 1 (2011).

[24] M. Hammen, W. Nörtershäuser, D. L. Balabanski, M. L. Bissell, K. Blaum, I. Budinčević, B. Cheal, K. T. Flanagan, N. Frömmgen, G. Georgiev, C. Geppert, M. Kowalska, K. Kreim, A. Krieger, W. Nazarewicz, R. Neugart, G. Neyens, J. Papuga, P.-G. Reinhard, M. M. Rajabali, S. Schmidt, D. T. Yordanov, B. Cheal, K. T. Flanagan, N. Frömmgen, G. Georgiev, C. Geppert, M. Kowalska, K. Kreim, A. Krieger, W. Nazarewicz, R. Neugart, G. Neyens, J. Papuga, P.-G. Reinhard, M. M. Rajabali, S. Schmidt, and D. T. Yordanov, Phys. Rev. Lett. **121**, 102501 (2018).

[25] D. T. Yordanov, L. V. Rodríguez, D. L. Balabanski, J. Bieroń, M. L. Bissell, K. Blaum, B. Cheal, J. Ekman, G. Gaigalas, R. F. Garcia Ruiz, G. Georgiev, W. Gins, M. R. Godefroid, C. Gorges, Z. Harman, H. Heylen, P. Jönsson, A. Kanellakopoulos, S. Kaufmann, C. H. Keitel, V. Lagaki, S. Lechner, B. Maaß, S. Malbrunot-Ettenauer, W. Nazarewicz, R. Neugart, G. Neyens, W. Nörtershäuser, N. S. Oreshkina, A. Papoulia, P. Pyykkö, P.-G. Reinhard, S. Sailer, R. Sánchez, S. Schiffmann, S. Schmidt, L. Wehner, C. Wraith, L. Xie, Z. Xu, and X. Yang, Commun. Phys. **3**, 107 (2020).

[26] W. G. Jiang, A. Ekström, C. Forssén, G. Hagen, G. R. Jansen, and T. Papenbrock, Phys. Rev. C **102**, 054301 (2020).

[27] S. Malbrunot-Ettenauer, S. Kaufmann, S. Bacca, C. Barbieri, J. Billowes, M. L. Bissell, K. Blaum, B. Cheal, T. Duguet, R. F. G. Ruiz, W. Gins, C. Gorges, G. Hagen, H. Heylen, J. D. Holt, G. R. Jansen, A. Kanellakopoulos, M. Kortelainen, T. Miyagi, P. Navrátil, W. Nazarewicz, R. Neugart, G. Neyens, W. Nörtershäuser, S. J. Novario, T. Papenbrock, T. Ratajczyk, P.-G. Reinhard, L. V. Rodríguez, R. Sánchez, S. Sailer, A. Schwenk, J. Simonis, V. Somà, S. R. Stroberg, L. Wehner, C. Wraith, L. Xie, Z. Y. Xu, X. F. Yang, and D. T. Yordanov, Phys. Rev. Lett. **128**, 022502 (2022).

[28] M. Kortelainen, Z. Sun, G. Hagen, W. Nazarewicz, T. Papenbrock, and P.-G. Reinhard, Phys. Rev. C **105**, L021303 (2022).

[29] B. K. Sahoo, A. R. Vernon, R. F. Garcia Ruiz, C. L. Binnersley, J. Billowes, M. L. Bissell, T. E. Cocolios, G. J. Farooq-Smith, K. T. Flanagan, W. Gins, R. P. de Groote, Á. Koszorús, G. Neyens, K. M. Lynch, F. Parnefjord-Gustafsson, C. M. Ricketts, K. D. A. Wendt, S. G. Wilkins, and X. F. Yang, New J. Phys. **22**, 012001 (2020).

[30] A. Vernon, R. de Groote, J. Billowes, C. Binnersley, T. Cocolios, G. Farooq-Smith, K. Flanagan, R. Garcia Ruiz, W. Gins, Á. Koszorús, G. Neyens, C. Ricketts, A. Smith, S. Wilkins, and X. Yang, Nucl. Instrum. Methods Phys. Res. B **463**, 384 (2020).

[31] A. R. Vernon, Evolution of the indium proton-hole states up to N = 82 studied with laser spectroscopy, Ph.D. thesis, University of Manchester, 2019, https://research.manchester.ac.uk/en/studentTheses/evolution-of-the-indium-proton-hole-states-up-to-n-82-studied-wit.

[32] C. L. Binnersley, Investigating the properties of multi-quasiparticle isomers in neutron-rich indium isotopes using laser spectroscopy, Ph.D. thesis, University of Manchester, 2019, https://research.manchester.ac.uk/en/studentTheses/investigating-the-properties-of-multi-quasiparticle-isomers-in-ne.

[33] C. M. Ricketts, Fundamental nuclear properties of indium isotopes measured with laser spectroscopy, Ph.D. thesis, University of Manchester, 2021, https://research.manchester.ac.uk/en/studentTheses/fundamental-nuclear-properties-of-indium-isotopes-measured-with-l.

[34] A. R. Vernon, C. M. Ricketts, J. Billowes, T. E. Cocolios, B. S. Cooper, K. T. Flanagan, R. F. Garcia Ruiz, F. P. Gustafsson, G. Neyens, H. A. Perrett, B. K. Sahoo, Q. Wang, F. J. Waso, and X. F. Yang, Sci. Rep. **10**, 12306 (2020).

[35] A. R. Vernon, R. F. Garcia Ruiz, T. Miyagi, C. L. Binnersley, J. Billowes, M. L. Bissell, J. Bonnard, T. E. Cocolios, J. Dobaczewski, G. J. Farooq-Smith, K. T. Flanagan, G. Georgiev, W. Gins, R. P. de Groote, R. Heinke, J. D. Holt, J. Hustings, Á. Koszorús, D. Leimbach, K. M. Lynch, G. Neyens, S. R. Stroberg, S. G. Wilkins, X. F. Yang, and D. T. Yordanov, Nature (London) **607**, 260 (2022).

[36] J. Karthein, C. M. Ricketts, R. F. Garcia Ruiz, J. Billowes, C. L. Binnersley, T. E. Cocolios, J. Dobaczewski, G. J. Farooq-Smith, K. T. Flanagan, G. Georgiev, W. Gins, R. P. de Groote, F. P. Gustafsson, J. D. Holt, A. Kanellakopoulos, Á. Koszorús, D. Leimbach, K. M. Lynch, T. Miyagi, W. Nazarewicz, G. Neyens, P. G. Reinhard, B. K. Sahoo, A. R. Vernon, S. G. Wilkins, X. F. Yang, and D. T. Yordanov, Nat. Phys. **20**, 1719 (2024).

[37] A. Vernon, C. Binnersley, R. Garcia Ruiz, K. Lynch, T. Miyagi, J. Billowes, M. Bissell, T. Cocolios, J. Delaroche, J. Dobaczewski, M. Dupuis, K. Flanagan, W. Gins, M. Girod, G. Georgiev, R. de Groote, J. D. Holt, J. Hustings, Á. Koszorús, D. Leimbach, J. Libert, W. Nazarewicz, G. Neyens, N. Pillet, P.-G. Reinhard, S. Rothe, B. Sahoo, S. R. Stroberg, S. Wilkins, X. Yang, Z. Xu, and D. Yordanov, companion paper, Phys. Rev. Lett. **134**, 252501 (2025).

[38] K. Lynch *et al.* (unpublished).

[39] J. Eberz, U. Dinger, G. Huber, H. Lochmann, R. Menges, R. Neugart, R. Kirchner, O. Klepper, T. Kühl, D. Marx, G. Ulm, and K. Wendt, Nucl. Phys. A **464**, 9 (1987).

[40] I. Dillmann, M. Hannawald, U. Köster, V. Fedoseyev, A. Wöhr, B. Pfeiffer, D. Fedorov, J. Shergur, L. Weissman, W. Walters, and K.-L. Kratz, Eur. Phys. J. A. **13**, 281 (2002).

[41] Á. Koszorús, J. Billowes, C. L. Binnersley, M. L. Bissell, T. E. Cocolios, B. S. Cooper, R. P. de Groote, G. J. Farooq-Smith, V. N. Fedosseev, K. T. Flanagan, S. Franchoo, R. F. Garcia Ruiz, W. Gins, K. M. Lynch, G. Neyens, F. P. Gustafsson, C. Ricketts, H. H. Stroke, A. Vernon, S. G. Wilkins, and X. F. Yang, Nucl. Instrum. Methods Phys. Res. B **463**, 398 (2020).

[42] S. Rothe, M. Au, J. Ballof, E. Barbero, M. Bissell, A. Boucherie, M. Bovigny, K. Chrysalidis, B. Crepieux, J. Cruikshank, E. Fadakis, R. Heinke, F. Josa, L. Le, A. Koliatos, E. Piselli, E. Reis, V. Samothrakis, M. Schütt, L. Lambert, D. Leimbach, S. Marzari, M. Owen, S. Stegemann, and Y.

Vila Gracia, Nucl. Instrum. Methods Phys. Res. B **542**, 38 (2023).
[43] S. Rothe, B. A. Marsh, C. Mattolat, V. N. Fedosseev, and K. Wendt, J. Phys.: Conf. Ser. **312**, 052020 (2011).
[44] E. Mané, J. Billowes, K. Blaum, P. Campbell, B. Cheal, P. Delahaye, K. T. Flanagan, D. H. Forest, H. Franberg, C. Geppert, T. Giles, A. Jokinen, M. Kowalska, R. Neugart, G. Neyens, W. Nörtershäuser, I. Podadera, G. Tungate, P. Vingerhoets, and D. T. Yordanov, Eur. Phys. J. A **42**, 503 (2009).
[45] A. Vernon, J. Billowes, C. Binnersley, M. Bissell, T. Cocolios, G. Farooq-Smith, K. Flanagan, R. Garcia Ruiz, W. Gins, R. de Groote, Á. Koszorús, K. Lynch, G. Neyens, C. Ricketts, K. Wendt, S. Wilkins, and X. Yang, Spectrochim. Acta B **153**, 61 (2019).
[46] V. Sonnenschein, I. D. Moore, S. Raeder, M. Reponen, H. Tomita, and K. Wendt, Laser Phys. **27**, 085701 (2017).
[47] M. Bass, P. A. Franken, A. E. Hill, C. W. Peters, and G. Weinreich, Phys. Rev. Lett. **8**, 18 (1962).
[48] W. Gins, R. de Groote, M. Bissell, C. Granados Buitrago, R. Ferrer, K. Lynch, G. Neyens, and S. Sels, Comput. Phys. Commun. **222**, 286 (2018).
[49] S. Stegemann, D. Atanasov, M. Au, E. Grenier-Boley, M. Butcher, M. Duraffourg, E. Fadakis, T. Feniet, Y. V. Gracia, T. Giles, J. Konki, L. Le, R. Lică, P. Martins, E. Matheson, C. Mihai, R. M. Muniz, C. Neacşu, G. Pascovici, K. Szczurek, S. Warren, and S. Rothe, Nucl. Instrum. Methods Phys. Res. B **541**, 169 (2023).
[50] M. Wang, W. Huang, F. Kondev, G. Audi, and S. Naimi, Chin. Phys. C **45**, 030003 (2021).
[51] F. Kondev, M. Wang, W. Huang, S. Naimi, and G. Audi, Chin. Phys. C **45**, 030001 (2021).
[52] A. Kramida, Y. Ralchenko, J. Reader, and NIST ASD Team, NIST Atomic Spectra Database (ver. 5.10), (online), available at `https://physics.nist.gov/asd` (21 September 2023), National Institute of Standards and Technology, Gaithersburg, MD (2023).
[53] I. Angeli and K. Marinova, At. Data Nucl. Data Tables **99**, 69 (2013).
[54] P. Klüpfel, P. G. Reinhard, T. J. Bürvenich, and J. A. Maruhn, Phys. Rev. C **79**, 034310 (2009).
[55] J. Dobaczewski, W. Nazarewicz, and P.-G. Reinhard, J. Phys. G: Nucl. Part. Phys. **41**, 074001 (2014).
[56] P.-G. Reinhard, B. Schuetrumpf, and J. Maruhn, Comput. Phys. Commun. **258**, 107603 (2021).
[57] P. Klüpfel, J. Erler, P.-G. Reinhard, and J. A. Maruhn, Eur. Phys. J. A **37**, 343 (2008).
[58] T. Miyagi, S. R. Stroberg, J. D. Holt, and N. Shimizu, Phys. Rev. C **102**, 034320 (2020).
[59] K. Hebeler, S. K. Bogner, R. J. Furnstahl, A. Nogga, and A. Schwenk, Phys. Rev. C **83**, 031301(R) (2011).
[60] J. Simonis, S. R. Stroberg, K. Hebeler, J. D. Holt, and A. Schwenk, Phys. Rev. C **96**, 014303 (2017).
[61] S. R. Stroberg, A. Calci, H. Hergert, J. D. Holt, S. K. Bogner, R. Roth, and A. Schwenk, Phys. Rev. Lett. **118**, 032502 (2017).
[62] T. Miyagi, S. R. Stroberg, P. Navrátil, K. Hebeler, and J. D. Holt, Phys. Rev. C **105**, 014302 (2022).
[63] J. Henderson, G. Hackman, P. Ruotsalainen, S. Stroberg, K. Launey, J. Holt, F. Ali, N. Bernier, M. Bentley, M. Bowry, R. Caballero-Folch, L. Evitts, R. Frederick, A. Garnsworthy, P. Garrett, B. Jigmeddorj, A. Kilic, J. Lassen, J. Measures, D. Muecher, B. Olaizola, E. O'Sullivan, O. Paetkau, J. Park, J. Smallcombe, C. Svensson, R. Wadsworth, and C. Wu, Phys. Lett. B **782**, 468 (2018).
[64] S. R. Stroberg, J. Henderson, G. Hackman, P. Ruotsalainen, G. Hagen, and J. D. Holt, Phys. Rev. C **105**, 034333 (2022).
[65] P.-G. Reinhard, J. O'Neal, S. M. Wild, and W. Nazarewicz, J. Phys. G **51**, 105101 (2024).
[66] A. Vernon for the CRIS Collaboration, "Dataset: Nuclear moments of indium isotopes reveal abrupt change at magic number 82 (2022)" [Data set], Zenodo, https://doi.org/10.5281/zenodo.6406949.
[67] J. Karthein for the CRIS Collaboration, "Dataset: Electromagnetic Properties of Indium Isotopes Elucidate the Doubly Magic Character of 100Sn (2023)" [Data set], Zenodo, https://doi.org/10.5281/zenodo.10138423.
[68] K. M. Lynch for the CRIS Collaboration, "Dataset: Variations in the charge radii of indium isotopes between N = 52 and 82 (2025)" [Data set], Zenodo, https://doi.org/10.5281/zenodo.15102530.